Significant Smartphone Images Features For Liver Steatosis Assessment

Khadidja Ould Amer, Baptiste Magnier, Stefan Janaqi, Manuela Cesaretti, Clément Labiche

Significant Smartphone Images Features For Liver Steatosis Assesment

Khadidja Ould Amer, Baptiste Magnier, Stefan Janaqi
EuroMov Digital Health in Motion,
Univ Montpellier, IMT Mines Ales,
Ales, France
{baptiste.magnier,stefan.janaqi}@mines-ales.fr

Manuela Cesaretti, Clement Labiche
Stella Surgical
5 Square de la poste
34920 Le Crès, France
{manuela.cesaretti,clement.labiche}@stellasurgical.com

***Abstract*—The growing demand for liver transplantation is leading medicine to explore new technologies in order to extend the field of viable transplants. Automatic hepatic steatosis assessment is the first step towards the development of a computer-aided liver diagnosis due to its importance as a risk factor for primary dysfunction. Color and texture are considered as two fundamental visual characteristics to assess the degree of hepatic steatosis. The aim of this study is to determine the discriminating features for liver image classification according to three steatosis classes: mild, moderate or severe. First, color features are extracted in three color spaces namely: RGB, HSV and YCbCr. Texture features are then extracted from RGB components using co-occurrence matrices, Local Binary Pattern (LBP) and Local Phase Quantization (LPQ). Additionally, feature-extraction was followed by generating a linear model regression using Least Absolute Shrinkage and Selection Operator (LASSO) allowing the classification task. The experimental results show that RGB histograms provide better classification accuracy. However, the relevance of these preliminary results is not sufficient to draw a decisive conclusion due to the experimental database, which is really small, very unbalanced and the images were captured under unknown and widely varying conditions.**

***Index Terms*—Liver images, histograms, texture, LASSO.**

I. Introduction and Context

Liver transplantation (LT) provides indisputable benefit for the survival and quality of life of patients with end-stage diseases [1]. The advances in liver transplantation medicine have led to its expansion over the past ten years. However, access to allografts remains the main limitation, because the growing number of patients who may benefit from the transplant consistently exceeds the number of organ donors. This issue has led to expand the liver selection criteria, which could have Hepatic Steatosis (HS), moving so the limit of acceptance for marginal livers. HS occurs initially by accumulation of triacylglycerols (TGs) in the cytoplasm of hepatocytes. It corresponds to the most important factors affecting liver allograft function and so LT outcome. Based on the size of hepatocytes TGs droplets, HS can be categorised as microvesicular or macrovesicular. Microvesicular has less influence on poor graft function than macrovesicular (MaS) which is one of the most important criteria defining the extended criteria of donor organs. Current quantification and grading of HS utilize a classification of mild (<33%), moderate (33%-66%), or severe (>66%) [2]. Mild MaS is considered a transplantable condition, whereas the use of donor livers with moderate MaS remains challenging. Grafts with severe steatosis (>60%) are highly recommended to be excluded, due to the critical risk of primary non-function.

Currently, the histological analysis of biopsied liver tissue performed during or after procurement is considered as the gold reference standard for the HS evaluation. However, this requires the availability of a cryostat facility and of an expert pathologist to interpret the result before or immediately after the liver retrieval. Consequently, this procedure can be invasive, time-consuming and difficult in a remote donor hospital. Due to the short time ailability between the liver procurement and its transplantation, the surgeons usually perform HS assessment through clinical evaluation (medical history, blood tests) and qualitative visual liver assessment [2]. The liver is evaluated in a standardized fashion according to certain criteria of parenchymal texture such as: yellowness, firmness and round liver edges. Fig. 1 shows two livers belonging to two different hepatic steatosis (HS) classes assessed by histopathological examination of liver tissue samples extracted with biopsy. Thus, liver with high percentage of steatosis (Fig.1(right)) is characterized by yellowish colors and more rounded edges than the liver in Fig.1(left) with mild hepatic steatosis (HS=5%). Such indicators can help surgeons to assess the overall liver quality for transplantation. Even if biopsy samples are taken, visual assessment of liver steatosis remains very important and always performed. However, it depends on the experience of the surgeon and becomes sometimes very difficult even for experienced surgeons [1]. In this context, the development of a simple, handy, fast and accurate device for non-invasive quantification of HS would obviously be most desirable.

As smartphones have become ubiquitous and the new generation ones are equipped by high resolution cameras, they could be the solution for automatic HS assessment. Indeed, the recent advances in computer vision has led to the development of various assisted diagnostics systems. In this context, texture and color are the fundamental characteristics used for optical images classification [3]–[5]. Inspired by these promising studies, the aim of this paper is to study different image descriptors in order to find the relevant characteristics allowing to predict the quality of the liver for transplantation and its limitations. This project represents the first attempt

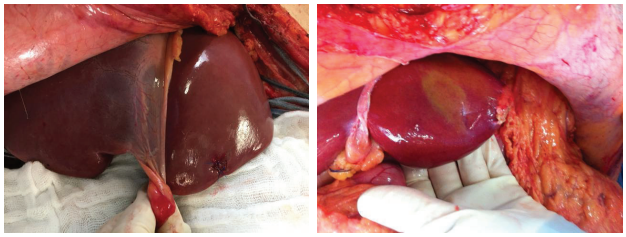

Fig. 1: Images of two livers acquired with smartphones in the operating room: liver with mild: HS=5% (left) and with severe hepatic steatosis: HS=85% (right).

to use automatic texture analysis of RGB (for Red Green and Blue channels) images and machine learning for graft HS assessment. The image database used in this study was initially introduced in the reaserch of Moccia *et al.* [6] on the same project. These images were acquired with different smartphones under different conditions wich include: a wide range of illumination, varying camera pose, different organ positions and presence of specular reflections. There is also the problem of image demosaicking [7] or image compression, degrading textures, colors and many details.

Features extraction consists to apply descriptors on the liver image. It is therefore interesting to know the precise region of the lobe in which the experts perform the biopsy. In this case, it makes more sense to apply the descriptors to the patch covering the region to be analyzed. However, the complete liver shape in many images of the database are not available. Consequently, the classification feasibility will be evaluated by applying both texture and color descriptors on the whole visible area of the liver in this study.

II. Texture descriptors

Texture analysis is a useful way whose primary purpose is to provide descriptors for image classification. In the medical field, texture-based information are increasingly used for computer aided diagnosis [6], [8], [9]. In this study, we focused on three commonly used texture descriptors: Co-occurrence matrices, Local Binary Pattern (LBP) and Local Phase Quantization (LPQ).

A. Gray Level Co-occurence Matrix (GLCM)

Grey Level Co-occurrence Matrix is one of the earliest methods used for image texture analysis [10]. This technique calculates the probability $P(i,j,d,\theta)$ which represents the number of times two pixels with gray level i and j appear at a relative distance d according to a given orientation θ:

$$P_{i,j}(d,\theta)=\#\{[(k,l)(m,n)\in(L_x,L_y)^2\,|\,I(k,l)=i,I(n,m)=j,d,\theta]\}, \tag{1}$$

where (k,l) and (m,n) are respectively, the coordinates of pixels i and j, $\#$ denotes the occurrence number of the pixel pair in the $(L_x \times L_y)$ image resolution cells ordered by their row-column designations. The conventionally used angular directions θ are 0, 45, 90 and 135 degrees. Note that $P(i,j,d,\theta)=P(j,i,d,\theta)$, thus GLCMs are a symmetric.

GLCMs provide a rich description of spatial dependence that is difficult to manipulate directly. Haralick *et al.* proposed a set of 14 statistical descriptors or attributes to summarize the textural information contained in the GLCMs [10]. However, only a subset of 5 descriptors are considered to be more relevant in the literature, namely: angular second moment or energy ENE, contrast CST, homogeneity HOM, entropy ENT and correlation COR are computed such as:

$$ENE=\sum_i\sum_j P_{i,j}(d,\theta)^2, \tag{2}$$

$$CST=\sum_i\sum_j (i-j)^2\cdot P_{i,j}(d,\theta), \tag{3}$$

$$HOM=-\sum_i\sum_j \frac{P_{i,j}(d,\theta)}{1+(i-j)^2}, \tag{4}$$

$$ENT=-\sum_i\sum_j P_{i,j}(d,\theta)\cdot\log(P_{ij}(d,\theta)), \tag{5}$$

$$COR=-\sum_i\sum_j P_{i,j}(d,\theta)\frac{(i-\mu_i)(j-\mu_j)}{\sqrt{\sigma_i^2\sigma_j^2}}, \tag{6}$$

where μ_i and σ_j represent the mean and standard deviation of the normalized inputs for the reference pixel i and neighbor pixel j respectively [10]. Also, $\mu_{\{i,j\}}$ and $\sigma_{\{i,j\}}$ correspond to $\mu_i=\sum_i i\cdot P_{i,j}$ and $\sigma_i=\sum_i P_{i,j}(i-\mu_i)^2$.

B. Local Binary Pattern (LBP)

The original version of the LBP labels the pixels by comparing each pixel with its 3×3-neighbourhood and considering the result as a binary number as illustrated in Fig. 2 [11]. The histogram of the labels is often used as a texture descriptor. The LBP operator was later generalized to deal with the texture at different scales by using neighborhoods of different sizes [12]. The thresholding function is defined as follows:

$$LBP_{P,R}=\sum_{p=0}^{P-1} s(g_p-g_c)\cdot 2^p, \quad \text{with } s(x)=\begin{cases}1 & x\geq 0\\ 0 & x<0,\end{cases} \tag{7}$$

where g_c and g_p are the gray level values of the central pixel and its neighbor respectively. P is the total number of the sampling points in a circular neighborhood of R radius around g_c.

The $LBP_{P,R}$ operator can produce 2^P different output values from the P neighbor pixels. Furthermore, the LBP operator rotation invariant $LBP^{ri}_{P,R}$ by assigning a unique label to each rotation invariant [13] (as an example, 01110000 and 00111000 are rotation invariant) is expressed by:

$$LBP^{ri}_{P,R}=min\,\{R_{OR}(LBP_{P,R},i)\,|\,i=0,1,...,P-1\}, \tag{8}$$

where $R_{OR}(x,i)$ performs a circular bit-wise right shift on the P-bit number x, i times.

Another extension of the LBP operator has been proposed to improve both the rotational invariance and to reduce the feature dimensionality. The uniform rotational invariance $LBP^{riu2}_{P,R}$ assigns an individual code to uniform patterns which contain at most 2 transitions (0 to 1 or vice versa) and a separate code to all non-uniform patterns. Its formal definition is given by the following equation:

$$LBP^{riu2}_{P,R}=\begin{cases}\sum_{p=0}^{P-1} s(g_p-g_c) & \text{if } U(LBP_{P,R})\leq 2\\ P+1 & \text{otherwise,}\end{cases} \tag{9}$$

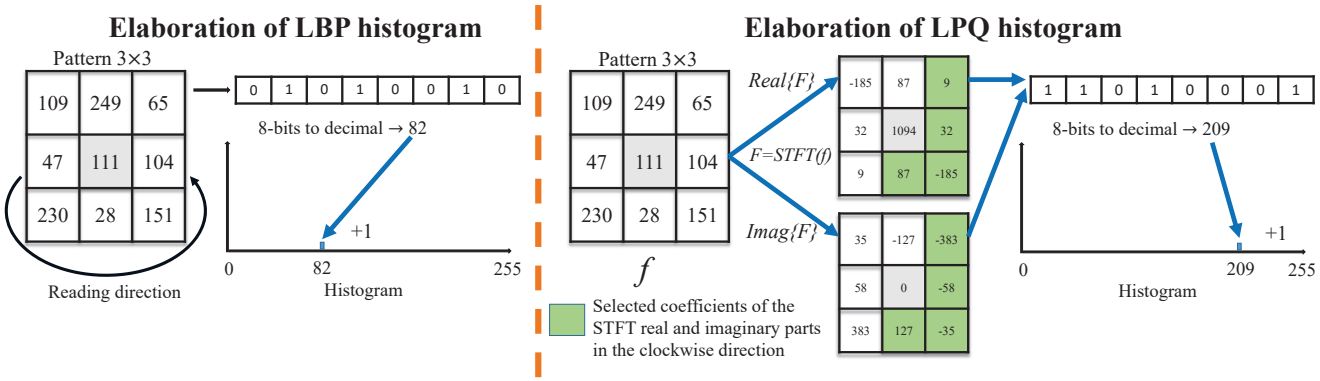

Fig. 2: Basic LBP and LPQ histogram calculation example.

where $U(LBP_{P,R})$ is computed as: $U(LBP_{P,R}) = |(s(g_{P-1} - g_c) - s(g_0 - g_c))| + \sum_{p=1}^{P-1} |(s(g_p - g_c) - s(g_{p-1} - g_c))|$. Thereafter, the $LBP^{riu2}_{P,R}$ operator is a texture descriptor by producing a histogram of $(P+2)$ bins.

C. Local Phase Quantization (LPQ)

The LPQ is blur invariant texture analysis method based on binary encoding of the phase information extracted from the 2-D short-term Fourier transform (STFT) computed over a local neighborhood at each pixel position of the image [14]. Thus, in digital image processing, the spatial blurring is represented by a convolution between the image intensity and a point spread function (PSF). In the Fourier domain, for given coefficient computed by the STFT u, this corresponds to: $G(u) = F(u) \cdot H(u)$, with G, F, and H represent the Fourier transforms of the blurred image, the original image, and the PSF respectively. By considering only the phase of the spectrum, the relation turns into a sum:

$$\angle G(u) = \angle F(u) + \angle H(u). \tag{10}$$

If the blur PSF is centrally symmetric, the Fourier transform $H(u)$ will always be real valued, and, as consequence: $\angle H(u) = 0$ if $H(u) \geq 0$, π otherwise. Furthermore, the shape of $H(u)$ for a regular PSF is close to a Gaussian or a sinc-function, which makes at least the low frequency values of $\angle H(u)$ to be positive [15]. Therefore, at these frequencies, $\angle G(u) = \angle F(u)$ causing $\angle F(u)$ to be a blur invariant. The LPQ method is based on this property of blur invariance. The local phase information is extracted using STFT computed over a rectangular neighborhood N_x of size $M \times M$ at each pixel position x of the image $f(x)$:

$$F(u, x) = \sum_{y \in N_x} f(x - y) e^{-j2\pi u^T y}. \tag{11}$$

Only four (more informative) complex coefficients are considered in LPQ, corresponding to: $u_1 = [a, 0]^T$, $u_2 = [0, a]^T$, $u_3 = [a, a]^T$, $u_4 = [a, -a]^T$, where a is small enough to satisfy $H(u) \geq 0$. This results in a 1×4 vector for each pixel position:

$$F_x = [F(u_1, x), F(u_2, x), F(u_3, x), F(u_4, x)]. \tag{12}$$

Finally, the phase information in the Fourier coefficients is recorded by observing the signs of the real and imaginary parts of each component in F_x as follows:

$$q_j(x) = \begin{cases} 1 & \text{if} \quad g_j(x) \geq 0 \\ 0 & \text{otherwise,} \end{cases} \tag{13}$$

where $g_j(x)$ is the j^{th} component of the vector $G_x = [Re\{F_x\}, Im\{F_x\}]$. The resulting eight binary coefficients $q_j(x)$ are represented as integer values between 0-255 using a binary encoding:

$$f_{LPQ}(x) = \sum_{j=1}^{8} q_j(x) \cdot 2^{j-1}. \tag{14}$$

Finally, as for the LBP descriptor (Fig. 2), the histogram of the label image f_{LPQ} is used as a 256-dimensional feature vector in classification.

An improved rotation-invariant local phase quantization (RI_LPQ) approach was proposed in [16]. This method consists of two steps: characteristic orientation estimation and directed descriptor extraction. Feature computation procedure is similar to the original LPQ, but the neighbourhood at each pixel location is rotated according to the direction of the characteristic orientation. Consequently, this technique (RI_LPQ) produces 256 features for a given grey level image and is compared in this study with previous descriptors.

III. Color Descriptors

Since hepatic steatosis causes a change in the color of the liver, color information becomes interesting features for image classification. Indeed, it has been demonstrated that considering the color in the image significantly improves the performance of many tasks in medical image analysis such as: melanoma detection [8] and skin lesions classification [17], [18]. Several color representations have been proposed to interpret the color information, each might outperform others in a particular application. This section introduces the commonly used color spaces in medical image analysis and presents the main texture descriptors trough these color spaces which are useful for the proposed study.

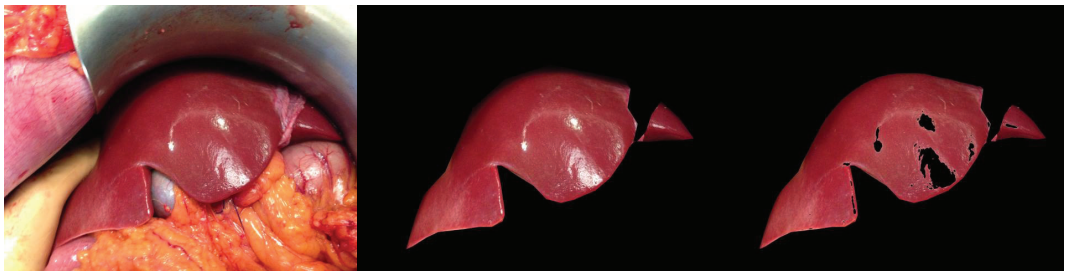

(a) Liver image (b) Manual segmentation (c) Specular reflections removed

Fig. 3: Liver image acquired by a surgeon smartphone.

A. Color Histogram Features

RGB is the default color space for storing and representing digital images. In this space, each color appears in its primary color components: Red, Green and Blue. There are many other color spaces that can be computed from the RGB space by means of linear or nonlinear transformations [19]. The HSV color space is closer to how humans perceive color in terms of: Hue (H), Saturation (S) and value (V). The hue component describes the wavelength of the color, saturation indicates the amount of white in the color and value represents the brightness which describes the intensity of light coming from the color. Several researches have used the HSV space to interpret the color information in color medical images. Indeed, the hue can reflect the abnormal appearance of tissues, saturation can be used to assess the level of abnormalities and value may indicates the property of luminance [20]. YCbCr is another color model which represents color. The Y in YCbCr signifies the luminance component while C_b and C_r represent the blue-difference and red-difference chroma components. YCbCr color model imitates human eye which is more sensitive to light intensity changes than hue changes. Therefore, the model allows to perceive more information from luminance and to obtain an efficient image representation [21].

Regardless of the used model, the distribution of intensities in each color channel is represented by a histogram of 256 bins (for images coded on 8 bits). These histograms can be concatenated and used as color descriptor of (3×256) values [17], [22]. Instead of concatenating the three histograms independently, it is also possible to generate a 3D histogram representing the joint distribution of the three channels. However, this increases the space dimensionality to 256^3 and an image quantization becomes necessary [8], [18].

B. Color and texture combination

Color and texture are two related characteristics of the image, but these characteristics are usually analyzed separately. Indeed, texture analysis methods are often applied to grayscale images for computational reasons and also for the interest of the intensity values of the pixels in the image. However, it has been demonstrated that texture features incorporating color information can improve the classification results. This generated two categories of methods:

- methods extracting color and texture features separately,
- methods considering color and texture jointly [23].

In the first approach, texture features extracted from the grayscale image are used in conjunction with other features describing the color distribution in a given color space [8], [9], [24]. For example, Riaz *et al.* [8] combine texture features extracted from GLCM with color histograms computed in three color space (including RGB and HSV) to classify the dermoscopy images into melanoma and non-melanoma. In the second approach, spatial and color distribution of pixels are jointly characterized by evaluating the texture features within each of the three color components independently [25], or by considering the spatial interactions within and between those components in a given color space [19].

In the following, the image classification is done in a first time by comparing histograms of concatenated color space channels (RGB, HSV, YCbCr), then by applying texture descriptors on the image in the most effective color space.

IV. Experiments and Results

A. Experimental Database

The database used in this study contains 154 RGB images, which refer to 154 different liver acquired with open-surgery view. As mentioned in the introduction, images were acquired with smartphones by surgeons under various conditions, which makes the classification task very challenging. Dataset images are divided into three classes according to HS rate assessed with biopsy. There is a significant imbalance between the classes: 125 images in class 1 $(HS \leq 30\%)$, referring to transplanted livers, 14 images in class 2 $(30 < HS \leq 50\%)$ corresponding to livers with moderate steatosis and 17 images in class 3 $(HS > 50\%)$ referred to discarded grafts with severe steatosis. Note that, these classes can be optionally changed depending on the expert decision.

Image analysis consists of applying the descriptors on the global area of the liver. Thus, manual segmentation was performed on each image to separate the liver organ from the background as shown in Fig. 3(a). Shadow areas and specular reflections were removed by setting to zero the bottom 'lowPercentile' and the top 'highPercentile' of all pixel values of the image, see Fig. 3(c).

	RGB			Cooccurrrence			HSV			YCbCr			LBP			LPQ		
	Act.1	**Act.2**	**Act.3**	**Act.1**	**Act.2**	**Act.3**	**Act.1**	**Act.2**	**Act.3**	**Act.1**	**Act.2**	**Act.3**	**Act.1**	**Act.2**	**Act.3**	**Act.1**	**Act.2**	**Act.3**
Predict. 1	25	1	3	20	3	2	22	3	0	18	3	2	23	3	2	22	3	3
Predict. 2	0	1	0	5	0	2	6	0	4	7	0	1	3	0	0	7	0	1
Predict. 3	5	1	1	5	0	0	2	0	0	5	0	1	4	0	2	1	0	0
	Metric			**Metric**			**Metric**			**Metric**			**Metric**			**Metric**		
	Se	**Sp**	**Acc**	**Se**	**Sp**	**Acc**	**Se**	**Sp**	**Acc**	**Se**	**Sp**	**Acc**	**Se**	**Sp**	**Acc**	**Se**	**Sp**	**Acc**
C1 vs C1C2	0.83	0.42	0.75	0.66	0.28	0.59	0.73	0.57	0.7	0.6	0.28	0.54	0.76	0.28	0.67	0.73	0.14	0.62
C2 vs C1C3	0.33	1	0.94	0	0.79	0.72	0	0.7	0.64	0	0.76	0.25	0	0.91	0.83	0	0.76	0.7
C3 vs C1C3	0.25	0.81	0.75	0	0.84	0.75	0	0.93	0.83	0.25	0.93	0.78	0	0.87	0.83	0	0.96	0.86
Mean	**0.47**	**0.74**	**0.81**	0.22	0.64	0.69	0.24	0.73	0.72	0.28	0.63	0.67	**0.42**	**0.69**	**0.78**	0.24	0.62	0.72

TABLE I: Performance measures for different color spaces and texture features.

B. Feature extraction

Image classification requires comparison of images according to a certain useful features. In this study, color and texture features were considered in order to find suitable representation for images. First, color features were extracted using color histograms in three color spaces namely: RGB, HSV, YCbCr. Indeed, the aim is to determine if a particular color space is optimum for our study.

Color content of the liver can be represented by a single 3D histogram or three separate 1D histograms. In a simplified way, for each color space, a feature vector is constructed by concatenating the corresponding three component histograms. We could have used the joint 3D histogram of the three channels since they are not statistically independent. However, this involves an image quantization to reduce the space dimensionality and thus a loss of information.

The differential structures in liver images may be analyzed with texture descriptors. In this study, spatial and color distribution of pixels were jointly characterized by evaluating texture features within each of the three color components (Red Green and Blue) of the image independently. Co-occurrence matrices were computed on these 3 channels separately using all the possible combinations of (θ, d), with $\theta \in \{0°, 45°, 90°, 135°\}$ and $d \in \{1, 2, 3\}$ (see eq. 1); then, the corresponding Haralick five features (ENE, CST, HOM, ENT and COR) were concatenated. On the other hand, $LBP^{P,R}_{riu2}$ (eq. 9) were then computed on each of the three channels: 10 features from $LBP^{1,8}_{riu2}$, 18 features from $LBP^{2,16}_{riu2}$ and 26 features from $LBP^{3,24}_{riu2}$, wich gives a total of $3 \times (10 + 18 + 26)$ LBP based features to a given image. Finally, rotation invariant RI_LPQ were computed over three neighborhood sizes ($M = 3; 5; 7$) and the corresponding histograms were concatenated. Note that the values of M were chosen to be consistent with the scales d and P used to calculate co-occurrence and LBP features, respectively. A total of $3 \times (256 \times 256)$ features were obtained by this method.

C. Classification with LASSO

Given a set of couples of observations $(x_k, y_k)_{k=\{1,....m\}}$, with $x_k \in \mathbb{R}^d$, a classical linear regression algorithm looks for a $w \in \mathbb{R}^d$ such that the predicting function $f(x, b, w) = b + w^T x$ fits the couple (x_k, y_k). Let $X \in \mathbb{R}^{(m \times d+1)}$ be the matrix with rows $[1, x_k^T]_{k=\{1,....m\}}$ and $w = [b, w]$. When the quality of fitting is measured by Euclidean distance, the optimal w is the solution of the optimization problem:

$$min\ \mathcal{L}(w) = \frac{1}{m} \parallel Xw - y \parallel_2^2, \tag{15}$$

where $\mathcal{L}$ is the loss function to be minimized. The d explaining features are the columns X_c of X with $c = 2, , d + 1$. When a budget of C features is given, the optimal w is the solution of:

$$min\ \mathcal{L}(w) = \frac{1}{m} \parallel Xw - y \parallel_2^2, \quad ||w||_0 \leqslant C. \tag{16}$$

Here, $||w||_0 = |\{c \mid w_c \neq 0, c \geq 2\}|$ (notice that $||w||_0$ is not a norm). The problem (eq. 16) arises also when the number of observations is less than the number of features $m<d$. Our problem falls into this case with $m \sim 10^2$ limited by the number of patients and $d \sim 10^3$ the number of numeric characteristics calculated from images. A main fact from linear algebra shows that the number of predicting features cannot be greater than $rank(X) \leqslant m$. Thus, one searches for a subset of $C \leqslant m$ features that give the best fit for y. The problem (eq. 16) is NP-hard and a good heuristic is to solve the following:

$$min\ \mathcal{L}(w) = \frac{1}{m} \parallel Xw - y \parallel_2^2, \quad ||w||_1 \leqslant K. \tag{17}$$

The minimization problem (eq.16) is LASSO (Least Absolute Shrinkage and Selection Operator) [26]:

$$min\ \mathcal{L}(w) = \frac{1}{2m} \parallel X_w - y \parallel_2^2 + \lambda \cdot ||w||_1. \tag{18}$$

This is a convex optimization problem that often finds sparse solutions w. In fact, the $\parallel * \parallel_1$-norm penalizing with the factor λ brings w_c to 0 whenever $corr(y, X_c) < \lambda$. The solution w gets sparser with increasing λ. Then, a trade-off can be easily found between the prediction error and the number of predicting features by controlling the sparsity of w through the penalizing factor λ.

To perform the classification, image database was divided into: a learning set (117 images) and a test set (37 images). Note that the learning set was created by randomly selecting 75% of images in each of the three classes while the remaining 25% were left to the test. For each of the features datasets, a learning model is constructed using LASSO classifier with the selected features. To evaluate the classification performance of the resulting models, sensitivity (Se), specificity (Sp) and accuracy (Acc) were compputed from the three confusion matrices (C1 vs C2C3), (C2 vs C1C3), (C3 vs C1C2):

$$Se = \frac{TP}{TP+FN}, \quad Sp = \frac{TN}{TN+FP}, \tag{19}$$

and

$$Acc = \frac{TP+TN}{TN+FP+TP+FN}, \quad (20)$$

where $C_{i,i\in\{1,2,3\}}$ are the three steatosis classes. Each row of the confusion matrices represents the instances in a predicted class while each column represents the instances in an actual (Act.) class. TP, TN, FP and FN represent the number of true positive, true negative, false positive and false negative, respectively.

The Tab. I reports all the classifications. In that respect, the best classification performance was obtained with the RGB dataset: (Se = 0.47, Sp = 0.74, Acc = 0.81). In this case, LASSO retains only 129 out of 3×256 features to drive features are really important to drive the correct predictions. However, by analysing the RGB confusion matrix, the sensitivity is decreased to (Se = 0.47) by the fact that the model correctly classified only one image of class 2 and 3. This problem is mainly due to the fact that we don't have enough images of classes 2 and 3 compared to class 1 in our database. This creates a significant imbalance between classes, reducing the model's ability to learn. For texture features, the results show that LBP perform better than co-occurrence and LPQ features with (Se = 0.42, Sp = 0.69, Acc = 0.78). However, there is no improvement compared to RGB results.

V. Conclusion

The aim of this study is to design a reliable model for automatic hepatic steatosis assessment. More specifically, we tried to answer the following question: which characteristics, texture or color, convey the most relevant information? The results showed that RGB histograms provide better classification accuracy. This contribution strengthens our claims that seeking specific descriptors might be the key for a future computer assisted system that can support surgeons to make the decision to accept or reject grafts. Future work should extend these results by using a larger and more balanced database for robust conclusions. Moreover, image acquisition needs to consider:

- camera pose
- organ position,
- color calibration of the imaging device,
- incoming illumination parameters influencing the color measurements.

Also, it would be interesting to combine the stronger color and texture feature set to increase the performance of the system.

References

[1] A. Martins, G.R. Coelho, G.A. Marques, J.T. Moraes, M.O.and Valença Jr, and José H.P. Garcia, "Hepatic steatosis assessment," *Arquivos de Gastroenterologia*, vol. 50, no. 1, pp. 15–18, 2013.

[2] M. Cesaretti, P. Addeo, L. Schiavo, R. Anty, and A. Iannelli, "Assessment of liver graft steatosis: Where do we stand?," *Liver Transplantation*, vol. 25, no. 3, pp. 500–509, 2019.

[3] R. Sumithra, M. Suhil, and D.S. Guru, "Segmentation and classification of skin lesions for disease diagnosis," *Procedia Computer Science*, vol. 45, pp. 76–85, 2015.

[4] Z. Abbas, M. Rehman, S. Najam, and S.M.D. Rizvi, "An efficient gray-level co-occurrence matrix (glcm) based approach towards classification of skin lesion," in *Amity Int. Conf. on Artificial Intelligence*. IEEE, 2019, pp. 317–320.

[5] H. Pang, T. Chen, X. Wang, Z. Chang, S. Shao, and J. Zhao, "Quantitative evaluation methods of skin condition based on texture feature parameters," *Saudi journal of biological sciences*, vol. 24, no. 3, pp. 514–518, 2017.

[6] S. Moccia, L.S. Mattos, I. Patrini, M. Ruperti, N. Poté, F. Dondero, F. Cauchy, A. Sepulveda, O. Soubrane, E. De Momi, et al., "Computer-assisted liver graft steatosis assessment via learning-based texture analysis," *Int. J. of Comp. Assisted Radiology and Surgery*, vol. 13, no. 9, pp. 1357–1367, 2018.

[7] Y. Yang O. Losson, L. Macaire, "Comparison of color demosaicing methods," *Adv. in Imaging and Electron Physics, Elsevier*, , no. 162, pp. 173–265, 2010.

[8] F. Riaz, A. Hassan, M. Y. Javed, and M. T. Coimbra, "Detecting melanoma in dermoscopy images using scale adaptive local binary patterns," in *Eng. in Med. and Bio. Soc.* IEEE, 2014, pp. 6758–6761.

[9] J.C. Kavitha and A. Suruliandi, "Texture and color feature extraction for classification of melanoma using svm," in *Comput. Tech. and Intell. Data Eng.* IEEE, 2016, pp. 1–6.

[10] R.M. Haralick, K. Shanmugam, and I.'H. Dinstein, "Textural features for image classification," *IEEE Transactions on systems, man, and cybernetics*, , no. 6, pp. 610–621, 1973.

[11] T. Ojala, M. Pietikäinen, and D. Harwood, "A comparative study of texture measures with classification based on featured distributions," *Patt. Rec.*, vol. 29, no. 1, pp. 51–59, 1996.

[12] T. Ojala, M. Pietikainen, and T. Maenpaa, "Multiresolution gray-scale and rotation invariant texture classification with local binary patterns," *TPAMI*, vol. 24, no. 7, pp. 971–987, 2002.

[13] M. Pietikäinen, T. Ojala, and Z. Xu, "Rotation-invariant texture classification using feature distributions," *Patt. Rec.*, vol. 33, no. 1, pp. 43–52, 2000.

[14] V. Ojansivu and J. Heikkilä, "Blur insensitive texture classification using local phase quantization," in *International conference on image and signal processing*. Springer, 2008, pp. 236–243.

[15] J. Heikkilä, E. Rahtu, and V. Ojansivu, "Local phase quantization for blur insensitive texture description," in *LBP: new variants and applications*, pp. 49–84. Springer, 2014.

[16] V. Ojansivu, E. Rahtu, and J. Heikkila, "Rotation invariant local phase quantization for blur insensitive texture analysis," in *ICPR*. IEEE, 2008, pp. 1–4.

[17] J.S. Marques, C. Barata, and T. Mendonca, "On the role of texture and color in the classification of dermoscopy images," in *Med. and Bio. Soc.* IEEE, 2012, pp. 4402–4405.

[18] M.A. Rahman, M.T. Haque, C. Shahnaz, S.A. Fattah, W.P. Zhu, and M. Ahmed, "Skin lesions classification based on color plane-histogram-image quality analysis features extracted from digital images," in *MWSCAS*. IEEE, 2017, pp. 1356–1359.

[19] Vinh Truong H., "Multi color space lbp-based feature selection for texture classification," Littoral, 2018.

[20] P.-H. Feng, Y.-T. Lin, and C.-M. Lo, "A machine learning texture model for classifying lung cancer subtypes using preliminary bronchoscopic findings," *Medical Physics*, vol. 45, no. 12, pp. 5509–5514, 2018.

[21] S. Soleimanizadeh, D. Mohamad, T. Saba, and A. Rehman, "Recognition of partially occluded objects based on the three different color spaces (rgb, ycbcr, hsv)," *3D Research*, vol. 6, no. 3, pp. 22, 2015.

[22] A.-A. Nahid and Y. Kong, "Histopathological breast-image classification using concatenated rgb histogram information," *Annals of Data Science*, vol. 6, no. 3, pp. 513–529, 2019.

[23] T. Mäenpää and M. Pietikäinen, "Classification with color and texture: jointly or separately?," *Patt. Rec.*, vol. 37, no. 8, pp. 1629–1640, 2004.

[24] O.R. Indriani, E.J. Kusuma, C.A. Sari, E.H. Rachmawanto, et al., "Tomatoes classification using k-nn based on glcm and hsv color space," in *ICITech*. IEEE, 2017, pp. 1–6.

[25] H. Ali, M.I. Lali, M.Z. Nawaz, M. Sharif, and B.A. Saleem, "Symptom based automated detection of citrus diseases using color histogram and textural descriptors," *Computers and Electronics in agriculture*, vol. 138, pp. 92–104, 2017.

[26] R. Tibshirani, "Regression shrinkage and selection via the lasso," *Journal of the Royal Statistical Society: Series B (Methodological)*, vol. 58, no. 1, pp. 267–288, 1996.